

Bilevel Fast Scene Adaptation for Low-Light Image Enhancement

Long Ma¹ · Dian Jin² · Nan An³ · Jinyuan Liu⁴ · Xin Fan¹ · Zhongxuan Luo³ · Risheng Liu¹

Received: date / Accepted: date

Abstract Enhancing images in low-light scenes is a challenging but widely concerned task in the computer vision. The mainstream learning-based methods mainly acquire the enhanced model by learning the data distribution from the specific scenes, causing poor adaptability (even failure) when meeting real-world scenarios that have never been encountered before. The main obstacle lies in the modeling conundrum from distribution discrepancy across different scenes. To remedy this, we first explore relationships between diverse low-light scenes based on statistical analysis, i.e., the network parameters of the encoder trained in different data distributions are close. We introduce the bilevel paradigm to model the above latent correspondence from the perspective of hyperparameter optimization. A bilevel learning framework is constructed to endow the scene-irrelevant generality of the encoder towards diverse scenes (i.e., freezing the encoder in the adaptation and testing phases). Further, we define a reinforced bilevel learning framework to provide a meta-initialization for scene-specific decoder to further ameliorate visual quality. Moreover, to improve the practicability, we establish a Retinex-induced architecture with adaptive denoising and apply our built learning framework to acquire its parameters by using two training losses including supervised and unsupervised forms. Extensive experimental evaluations on multiple datasets verify our adapt-

ability and competitive performance against existing state-of-the-art works. The code and datasets will be available at <https://github.com/vis-opt-group/BL>.

Keywords Low-light image enhancement, image denoising, fast adaptation, bilevel optimization, hyperparameter optimization, meta learning

1 Introduction

Images captured in low-light conditions tend to appear problems like poor contrast and high noise, which seriously affect image quality. Unfortunately, there are many inevitable challenging shooting conditions. Low-light images reduce the visual quality as well as hinder the following industrial application content. Specifically, it affects some high-level tasks, e.g. detection (Wang et al. 2022; Liang et al. 2021b; Cui et al. 2021), segmentation (Wu et al. 2021; Sakaridis et al. 2019; Gao et al. 2022a) and tracking (Ye et al. 2022). Therefore, the study of low-light image enhancement has strong practical significance.

Benefiting from the flourishing development of Convolutional Neural Networks (CNNs) (Gu et al. 2018), constructing CNNs for low-light image enhancement (Chen et al. 2018; Zhang et al. 2019; Ma et al. 2022) has become the principal measure. Data is the foundation stone for learning a CNN model and can be divided into with and without reference images, corresponding to the supervised (Xu et al. 2020; Zheng et al. 2021) and unsupervised (Li et al. 2021; Jiang et al. 2021) learning paradigms which are two patterns in CNN-based low-light image enhancement. However, a common issue with these existing techniques is that they are just effective enough for images that possess a similar distribution to the training dataset since the regular end-to-end learning paradigm. It causes that these works usually need to spend too much energy in learning a completely

Corresponding author: Risheng Liu
E-mail: rsliu@dlut.edu.cn

¹ DUT-RU International School of Information Science & Engineering, Dalian University of Technology, Dalian, 116024, China.

² Xiaomi AI Lab, Beijing, 100085, China.

³ School of Software Technology, Dalian University of Technology, Dalian, 116024, China.

⁴ School of Mechanical Engineering, Dalian University of Technology, Dalian, 116024, China.



Fig. 1 Visual comparison among two representative recently-proposed methods (including FIDE (Xu et al. 2020) and SCL (Liang et al. 2022)) and our proposed algorithm on four different benchmarks (including MIT (Bychkovsky et al. 2011b), LOL (Chen et al. 2018), VOC (Lv et al. 2021), ExDark (Loh and Chan 2018)). Obviously, our method realizes the best visual quality on all challenging scenarios.

new model for unseen low-light scenes. In other words, they have a limited solving capacity and cannot adapt to other low-light scenes quickly and effectively.

To endow the fast adaptation for the learned model, a series of works (Lee et al. 2020; Park et al. 2020; Chi et al. 2021) based on meta-learning (Finn et al. 2017) have been developed for different low-level vision tasks (*have not been investigated in the field of low-light image enhancement*). Most of them explicitly define meta-initialization (Liu et al. 2021a) learning as the pathway to realizing fast adaptation. Meta-initialization learning is to acquire a general initialization of network parameters from multiple tasks, then just perform the fine-tuning process when meeting the new task. Indeed, these works perform a fast adaptation ability towards new tasks (commonly defined as the new scene that never encountered before). However, the above approach of achieving fast adaptation is just to connect multiple tasks from the initial status, ignoring the unified representation in the feature space to abandon the opportunity of a shortcut for fast adaptation.

In this work, we develop a new bilevel learning scheme for fast adaptation by bridging the gap between low-light scenes in the learning procedure. As shown in Fig. 1, we can easily observe that our proposed method realizes the best visual quality on different challenging scenarios against other advanced methods. It indicates that we indeed achieve the goal of adapting scenarios. Our main contributions can be concluded as the following five-folds.

- To the best of our knowledge, we are the first to focus on fast adaptation for low-light image enhancement from the view of hyperparameter optimization, to ameliorate the adaptability towards unknown scenes.
- We propose to use bilevel paradigm to model the latent scene-irrelevant correspondence which presents that the parameters are close between encoders trained in different data distributions based on statistical exploration.
- We design a new Bilevel Learning (BL) framework to learn a scene-irrelevant encoder for freezing its parameters when meeting unknown scenes. It reduces training costs to support fast adaptation nicely.

- Considering the indefinite initialization of scene-specific decoder, we establish a Reinforced Bilevel Learning (RBL) framework to provide a meta-initialization to further improve adapting efficiency.
- To handle different challenging scenes, we build a new Retinex-induced encoder-decoder architecture with an adaptive denoising mechanism and define two training patterns including supervised and unsupervised forms.

This work is extended from our preliminary version (Jin et al. 2021) with the promotion from three key aspects.

- We provide an elaborate analysis about the research motivation by presenting the distribution discrepancy and exchanging learned architectures.
- We develop a reinforced bilevel learning to energizing the initialization of the scene-specific decoder for further improving performances.
- Sufficient comparisons on more benchmarks with recent advanced methods and detailed analyses are performed to prove our effectiveness.

2 Related Works

In this part, we make a comprehensive review of related works including CNNs for low-light image enhancement, and fast adaptation for low-level vision.

CNNs for low-light image enhancement. Recently, accounting for the rapid development of deep learning, advanced algorithms in the field of low-light image enhancement continued to emerge. Many CNN-based methods have achieved surprising results in low-light image enhancement. According to different learning patterns with different scene adaptation abilities, existing works can be roughly divided into two categories: supervised and unsupervised learning.

Supervised learning is the most common paradigm which benefits from the development of the paired low-/normal-light datasets (e.g., LOL (Chen et al. 2018), MIT (Bychkovsky et al. 2011a), LSRW (Hai et al. 2021), and VOC (Lv et al. 2021)). RetinexNet (Chen et al. 2018) provided an end-to-end framework that combined Retinex theory with deep net-

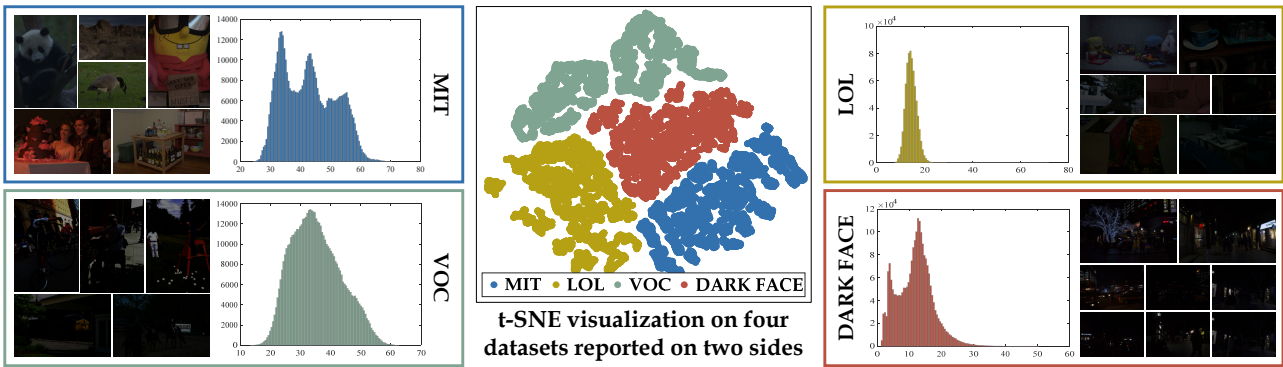


Fig. 2 Demonstrating distribution discrepancy of different datasets. On two sides, we randomly sampled 100 low-light images each from four datasets to plot the histogram. The middle subfigure plots the t-SNE distribution (Van der Maaten and Hinton 2008) on these four datasets.

works. KinD (Zhang et al. 2019) adjusted RetinexNet to estimate the illumination and added a series of training losses. DeepUPE (Wang et al. 2019a) could adapt to the complex illumination of the ground truth by learning the mapping between low-light images and illumination. FIDE (Xu et al. 2020) proposed to restore image objects in the low-frequency layer, and enhanced high-frequency details on the restored image. DSNNet (Zhao et al. 2021) developed a symmetrical deep network by combining an invertible feature transformer and two pairs of pre-trained encoder-decoder. The work in (Zheng et al. 2021) proposed an adaptive unfolding total variation network to realize noise reduction and detail preservation. Wu et al. (Wu et al. 2022) designed a URetinex-Net by unfolding the Retinex-based optimization and learning data-dependent priors. DCC-Net (Zhang et al. 2022) followed the “divide and conquer” collaborative strategy to construct a deep color consistent network by separately restoring gray images and color distribution. However, limited to the specific distribution from the paired data, the main drawback of this paradigm is the generalization capabilities of models.

Unsupervised learning focuses on learning the model without the support of data with reference. EnGAN (Jiang et al. 2021) first raised that unpaired training scheme based on generative-adversarial mode could be introduced into low-light image enhancement, which enhanced the generalization performance of the algorithm to a certain extent. Nevertheless, it was unstable and prone to tail shadow and color bias. The work in (Ma et al. 2021) constructed a context-sensitive decomposition network and also adopted the pattern of generative-adversarial. ZeroDCE (Guo et al. 2020), an unsupervised method, designed a lightweight deep network to estimate pixels and high-order curves for dynamic range adjustment of a given image. However, introducing a series of training losses weakened the excellent generalization of the unsupervised learning without the paired/unpaired data. The work in (Liang et al. 2021a) developed a semantically contrastive learning mechanism by three constraints

of contrastive learning, semantic brightness consistency, and feature preservation to guarantee the consistencies of color, texture, and exposure. Ma et al. (Ma et al. 2022) built a self-calibrated illumination learning framework for unsupervised low-light image enhancement.

In summary, most above-mentioned low-light image enhancement algorithms were still addressing one or some specific issues in one single scene from the training dataset. They are difficult to adapt to other challenging scenes which contain unseen distributions. In other words, the similarities and differences between various scenes should be exploited fully to improve the model’s generalization.

Fast adaptation for low-level vision. Currently, the adaptability of models in different scenes has received unprecedented attention. Methods with fast adaptation and less training costs are becoming more and more popular. The emergent meta-learning (Wang et al. 2021; Vuorio et al. 2019; Liu et al. 2021a; Gao et al. 2022b) has attracted broad attention in various fields on the strength of powerful ability of “learning to learn”. Especially, the popular Model-Agnostic Meta-Learning (MAML) (Finn et al. 2017) learns the meta-initialization from multiple tasks to receive a fast adaptation property towards the new task, which has been widely applied to low-level vision field to realize the fast adaptation.

Lee et al. (Lee et al. 2020) combined the internal statistics of a natural image used for exploiting the self-similarity, and a MAML-based meta-learning paradigm to construct a fast adaptation denoising algorithm. The paper in (Park et al. 2020) applied the meta-learning for super-resolution and utilized the patch-recurrence property of the natural image to boost the performance. The work in (Chi et al. 2021) introduced a self-reconstruction auxiliary task for primary deblurring and designed the meta-auxiliary learning to endow the fast adaptation ability for dynamic scene deblurring. To solve the difficulty of learning a general dehazing model on multiple datasets, a multi-domain learning approach for dehazing was constructed in (Liu et al. 2022) by designing the helper network for boosting the performance during the test

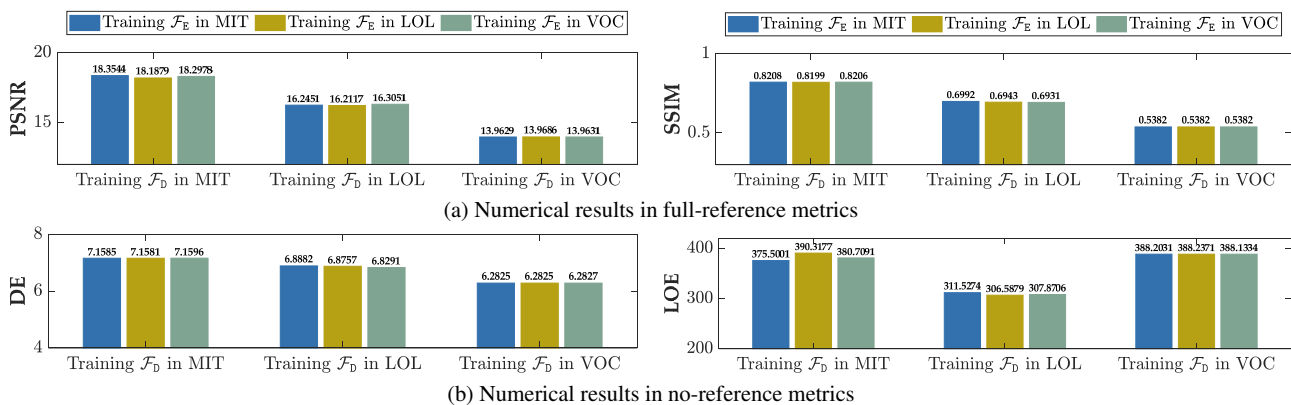


Fig. 3 Quantitative scores after exchanging the encoder and decoder trained in different datasets. Note that the testing dataset for each case is the same one used in training \mathcal{F}_D .

time and introducing the meta-learning paradigm to intensify the generality of the helper network. Choi *et al.* (Choi *et al.* 2021) proved that the meta-learning framework could be easily applied to any video frame interpolation network with only a few fine-tunings.

Although many low-level vision fields had begun to consider the problem of model generalization capabilities as described above, because of the diversity of low-light scenes, the low-light image enhancement field never had a good application in this regard.

3 Exploring Relationships among Low-Light Scenes

Here, we explore the relationship between diverse low-light data distributions from two aspects. On one hand, we first present the difference among diverse datasets from a statistical perspective. On the other hand, we excavate the latent relationship among datasets from the trained model.

We know that the low-light scenes are miscellaneous including the appearance, level of luminance, and so on. Here we consider four different datasets including MIT (Bychkovsky *et al.* 2011b), LOL (Chen *et al.* 2018), VOC (Lv *et al.* 2021), and DARK FACE (Yang *et al.* 2020). They are with different objects, scenes, and levels of luminance. As shown in Fig. 2, we plot the low-light examples and distribution for these datasets, and their relationship in the same dimension. There exists an apparent distribution discrepancy between these datasets, that is to say, it is extremely difficult to establish a unified model for adapting them. It actually reveals why most of existing works need to retrain their whole model in the unseen scenes.

A question worth pondering is whether there exists one possibility to bridge these various datasets. Here we would like to explore the relationship among models trained by different datasets. We define the enhancement architecture as

an encoder-decoder¹ architecture (Ronneberger *et al.* 2015), formulated as $\mathcal{F} = \mathcal{F}_E \cup \mathcal{F}_D$ (\mathcal{F} : encoder-decoder, \mathcal{F}_E : encoder, and \mathcal{F}_D : decoder). We adopt three various datasets (including MIT, LOL, and VOC) presented in Fig. 2 to analyze this process.

To be concrete, we first train three distribution-specific models on all these datasets. We adopt the MSE loss to train it and the numbers of training and testing samples follow the settings of the adaptation stage in Table 1. In the testing phase for the specific dataset (e.g., MIT), we perform the results of three versions including the original model trained on MIT, and the other two models by substituting the original encoder as the trained on other datasets (i.e., LOL and VOC). By performing this procedure on these three datasets and calculating four metrics consisting of two full-reference metrics (i.e., PSNR and SSIM), and two no-reference metrics (i.e., DE (Shannon 1948) and LOE (Wang *et al.* 2013)), we plot these numerical results in Fig. 3. Evidently, although the encoder and decoder are not trained in the same dataset, these scores on different settings all approach the same state. That is to say, the encoder has a unified representation that is scene-irrelevant.

Actually, the phenomenon above manifests there exists a pattern to alleviate the transferred burden towards unseen distributions. It exactly coincides with the goal of fast adaptation in the field of low-level vision (Choi *et al.* 2021; Liu *et al.* 2022). However, a substantive difference lies in the regular fast adaptation mostly learns a meta-initialization based on the meta-learning mechanism (Lee *et al.* 2020; Park *et al.* 2020; Choi *et al.* 2021; Liu *et al.* 2022), i.e., *all parameters need to be finetuned when applied to unknown scenes, see Fig. 4 (a)*. Different from it, our finding above is to provide a generic encoder whose parameters are frozen when meeting unknown scenes, i.e., *part of parameters are frozen, and rest need to be finetuned, see Fig. 4 (b)*. Briefly,

¹ More details can be found in Sec. 5.

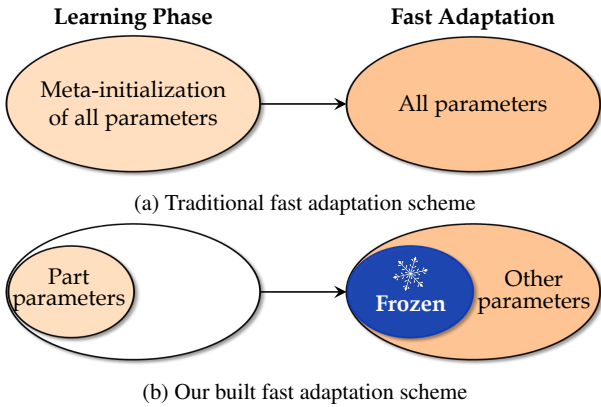


Fig. 4 Comparing different fast adaptation schemes. (a) represents the traditional scheme (Lee et al. 2020; Park et al. 2020; Choi et al. 2021; Liu et al. 2022) based on meta-learning for fast adaptation. (b) is our built fast adaptation scheme based on bilevel learning. In contrast, the latter can largely reduce the computational burden in the adaptation stage by just fine-tuning part parameters, rather than all parameters.

the desired fast adaptation ability is more challenging than traditional fast adaptation.

In the following, based on the observations above, we introduce bilevel learning for fast adaptation to improve the model generality and reduce the burden of transferring.

4 Fast Adaptation via Bilevel Learning

This section first provides a modeling perspective from hyperparameter optimization for fast adaptation among diverse datasets, then constructs a bilevel learning scheme and its reinforced version for handling the built model.

4.1 Modeling with Bilevel Paradigm

In essence, many vision problems can be modeled as the specific optimization model. Fortunately, our desired fast adaptation scheme shown in Fig. 4 (b) can be exactly presented as the hyperparameter optimization. Hyperparameter optimization (Feurer and Hutter 2019; Falkner et al. 2018; Liu et al. 2021a) is an emergent concept, which is defined as *finding a tuple of hyperparameters that yields an optimal model which minimizes a predefined loss function on given independent data*². In our designed scheme, the parameters in the learning phase can be viewed as the hyperparameters, and the other parameters can be viewed as the parameters. Then the hyperparameter optimization can be written as the following bilevel model

$$\begin{aligned} \min_{\mathbf{u} \in \mathcal{U}} F(\mathbf{u}, \mathbf{v}; \mathcal{D}_{\text{val}}), \\ \text{s.t. } \mathbf{v} \in \mathcal{S}(\mathbf{u}), \mathcal{S}(\mathbf{u}) := \arg \min_{\mathbf{v}} f(\mathbf{u}, \mathbf{v}; \mathcal{D}_{\text{tr}}), \end{aligned} \quad (1)$$

² https://en.wikipedia.org/wiki/Hyperparameter_optimization.

where \mathbf{u} and \mathbf{v} represent the hyperparameters and parameters, respectively. $\mathcal{S}(\mathbf{u})$ is the set of solution of the lower-level problem. $F(\cdot)$ and $f(\cdot)$ are the objective for the upper and lower level, respectively. $\mathcal{D} = \mathcal{D}_{\text{tr}} \cup \mathcal{D}_{\text{val}}$ denotes that the given dataset \mathcal{D} is split into the training set \mathcal{D}_{tr} and validation set \mathcal{D}_{val} . Eq. (1) actually presents an explicit relationship between hyperparameters and parameters.

From the perspective of hyperparameter optimization, we hope to obtain a fast adaptation ability by defining a hyper-network that consists of hyperparameters in our designed architecture. To be specific, we know that the encoder extracts features from diverse inputs, and the decoder reconstructs features to output the desired targets. Actually, these features between encoder and decoder are compactly relevant to low-light inputs, that is to say, the encoder characterizes the representation of diverse inputs from different scenarios. The results reported in Fig. 3 can also verify the observation. Additionally, inspired by the work in (Franceschi et al. 2018), here we define the encoder as the scene-irrelevant hyper-network that learns the hyperparameter in Eq. (1). Then the decoder can be viewed as a scene-specific network, which learns the parameters in Eq. (1). This procedure presents that

$$\mathbf{u} = \Theta_{\mathcal{F}_E}, \mathbf{v} = \Theta_{\mathcal{F}_D}, \quad (2)$$

where $\mathcal{F} = \mathcal{F}_E \cup \mathcal{F}_D$ represents the Retinex-induced encoder-decoder³. \mathcal{F} consists of encoder \mathcal{F}_E and decoder \mathcal{F}_D . As for the definition of F and f , we adopt our defined loss for Retinex-induced encoder-decoder described in the above.

In this way, we can successfully model our designed architecture by using the bilevel model based on hyperparameter optimization, to acquire the ability of fast adaptation. How to solve it become our next concentration.

4.2 Bilevel Learning Framework

As for solving Eq. (1), on one hand, it has been proved that the bilevel optimization model is extremely complex and difficult to solve (Franceschi et al. 2018; Liu et al. 2020b). Even though we can utilize the existing solving scheme (Liu et al. 2020b, 2021b, 2020a) for the bilevel model to solve our model. But it needs to consume a huge computational burden. This is why existing bilevel techniques just can be applied to some simple tasks, e.g., few-shot learning (Simon et al. 2020; Ziko et al. 2020).

To solve Eq. (1) efficiently, following the solving manner for neural architecture search as presented in (Liu et al. 2018), we adopt a simple approximation scheme to solve it, formulated as

$$\nabla_{\mathbf{u}} F(\mathbf{u}, \mathbf{v}; \mathcal{D}_{\text{val}}) \approx \nabla_{\mathbf{u}} F(\mathbf{u}, \mathbf{v} - \xi \nabla_{\mathbf{v}} f(\mathbf{u}, \mathbf{v}; \mathcal{D}_{\text{tr}}); \mathcal{D}_{\text{val}}),$$

³ More details can be found in Sec. 5.

(3)

where ξ is a learning rate for a step of lower-level optimization. This way is to approximate the hyperparameter \mathbf{u} using only a single training step, without solving lower-level problem accurately.

Furthermore, an inevitable phenomenon is that the second order gradient will appear after applying the chain rule, formulated as

$$\nabla_{\mathbf{u}} F(\mathbf{u}, \mathbf{v}'; \mathcal{D}_{\text{val}}) - \xi \nabla_{\mathbf{u}, \mathbf{v}}^2 f(\mathbf{u}, \mathbf{v}; \mathcal{D}_{\text{tr}}) \nabla_{\mathbf{v}'} F(\mathbf{u}, \mathbf{v}'; \mathcal{D}_{\text{val}}), \quad (4)$$

where $\mathbf{v}' = \mathbf{v} - \xi \nabla_{\mathbf{v}} f(\mathbf{u}, \mathbf{v}; \mathcal{D}_{\text{tr}})$ denotes the weights for a one-step forward model. In the above equation, there appears an expensive matrix-vector product which increases the complexity for this formulation. Fortunately, it can be substantially reduced by using the finite difference approximation, expressed as

$$\begin{aligned} & \nabla_{\mathbf{u}, \mathbf{v}}^2 f(\mathbf{u}, \mathbf{v}; \mathcal{D}_{\text{tr}}) \nabla_{\mathbf{v}'} F(\mathbf{u}, \mathbf{v}'; \mathcal{D}_{\text{val}}), \\ & \approx \frac{\nabla_{\mathbf{u}} f(\mathbf{u}, \mathbf{v}^+; \mathcal{D}_{\text{tr}}) - \nabla_{\mathbf{u}} f(\mathbf{u}, \mathbf{v}^-; \mathcal{D}_{\text{tr}})}{2\epsilon}, \end{aligned} \quad (5)$$

where ϵ is a small constant, $\mathbf{v}^{\pm} = \mathbf{v} \pm \epsilon \nabla_{\mathbf{v}'} F(\mathbf{u}, \mathbf{v}'; \mathcal{D}_{\text{val}})$. In this way, solving Eq. (4) requires only two forward passes for the weights and two backward passes for \mathbf{u} .

In general, our established bilevel learning strategy contains three stages, i.e., learning scene-irrelevant encoder, fast adaptation to the scene that has never been encountered before, and testing process.

4.3 Reinforced Bilevel Learning Framework

Indeed, our above-built bilevel learning paradigm has satisfied the demand for fast adaptation by learning a scene-irrelevant encoder, but an inevitable issue is that the decoder needs to learn from scratch in the fast adaptation stage, leading to the adaptation difficulty. That is to say, can we provide a better, unified initialization for the decoder to adapt to various scenes better?

Following the work in (Liu et al. 2021c,a), here we introduce the meta-initialization process $\tilde{\mathbf{v}} = \Theta_{\mathcal{F}_D}^0$, to impose the meta-learning ability to decoder in the bilevel learning phase. To be specific, we define the following bilevel optimization

$$\begin{aligned} & \min_{\tilde{\mathbf{v}} \in \mathcal{V}} H(\tilde{\mathbf{v}}, \mathbf{v}; \mathcal{D}_{\text{val}}), \\ & \text{s.t. } \mathbf{v} \in \mathcal{R}(\tilde{\mathbf{v}}), \mathcal{R}(\tilde{\mathbf{v}}) := \arg \min_{\tilde{\mathbf{v}}} h(\tilde{\mathbf{v}}, \mathbf{v}; \mathcal{D}_{\text{tr}}), \end{aligned} \quad (6)$$

where $H(\cdot)$ and $h(\cdot)$ keep the same meaning with $F(\cdot)$ and $f(\cdot)$, respectively. $\mathcal{R}(\tilde{\mathbf{v}})$ is the set of solution of the lower-level problem. Actually, the above-built model has the same

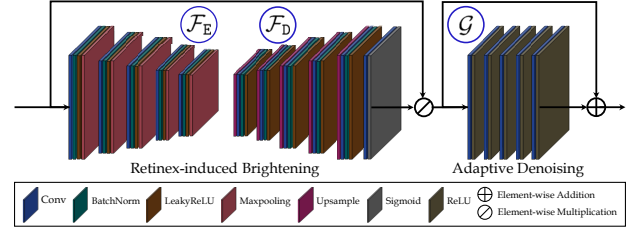


Fig. 5 The overall network architecture, which contains Retinex-induced brightening and adaptive denoising. The rectangle box below shows the operations used in our constructed architecture.

form as Eq. (1), that is to say, we can use the same solving strategy for this model. It can be formulated as

$$\begin{aligned} & \nabla_{\tilde{\mathbf{v}}} H(\tilde{\mathbf{v}}, \mathbf{v}; \mathcal{D}_{\text{val}}) \approx \\ & \nabla_{\tilde{\mathbf{v}}} H(\tilde{\mathbf{v}}, \mathbf{v}'; \mathcal{D}_{\text{val}}) - \frac{\nabla_{\tilde{\mathbf{v}}} h(\tilde{\mathbf{v}}, \mathbf{v}^+; \mathcal{D}_{\text{tr}}) - \nabla_{\tilde{\mathbf{v}}} h(\tilde{\mathbf{v}}, \mathbf{v}^-; \mathcal{D}_{\text{tr}})}{2\epsilon}, \end{aligned} \quad (7)$$

where $\mathbf{v}' = \mathbf{v} - \xi \nabla_{\mathbf{v}} h(\tilde{\mathbf{v}}, \mathbf{v}; \mathcal{D}_{\text{tr}})$, $\mathbf{v}^{\pm} = \mathbf{v} \pm \epsilon \nabla_{\mathbf{v}'} H(\tilde{\mathbf{v}}, \mathbf{v}'; \mathcal{D}_{\text{val}})$, ϵ is a small constant.

5 Network Architecture and Training Loss

In this section, we introduce a Retinex-induced brightening to satisfy the task demand according to the domain knowledge. Then we construct a new adaptive denoising mechanism to handle the noises. Finally, we introduce the training loss for these two parts.

5.1 Retinex-induced Brightening Architecture

Retinex theory (Land and McCann 1971) is the well-known and commonly-approved model for low-light image enhancement. This theory says that a given low-light image can be decomposed as the illumination and reflectance. The formulation can be written as $\mathbf{y} = \mathbf{x} \odot \mathbf{z}$, where \mathbf{y} , \mathbf{x} , and \mathbf{z} represent the low-light observation, illumination, and reflectance, respectively. \odot is the element-wise multiplication. As described in existing works (Guo et al. 2017; Zhang et al. 2018a), the illumination component is the key for addressing this task. Following the consensus, we establish a direct mapping between low-light and normal-light image as

$$\begin{cases} \mathbf{x} = \mathcal{F}(\mathbf{y}; \Theta_{\mathcal{F}}), \\ \mathbf{z} = \mathbf{y} \oslash \mathbf{x}, \end{cases} \quad (8)$$

where $\mathcal{F} = \mathcal{F}_E \cup \mathcal{F}_D$ represents the Retinex-induced encoder-decoder (Ronneberger et al. 2015) consists of encoder \mathcal{F}_E and decoder \mathcal{F}_D with the parameters $\Theta_{\mathcal{F}}$ to convert the low-light input to illumination. \oslash denotes the element-wise division operation. In this way, we successfully perform domain

Table 1 Benchmarks description.

Benchmarks	Seen-paired		Unseen-paired		Unseen-unpaired
	MIT	LOL	LSRW	VOC	DARKFACE
Learning	✓	✓	×	×	×
(Numbers)	(500)	(500)	(—)	(—)	(—)
Adaptation	✓	✓	✓	✓	✓
(Numbers)	(500)	(500)	(500)	(500)	(500)
Testing	✓	✓	✓	✓	✓
(Numbers)	(100)	(100)	(50)	(100)	(100)

knowledge in the network design to obtain the basic performance support.

As for the architecture of encoder-decoder, the encoder consists of four down-sampling steps and a block (i.e. a convolutional layer, a batch normalization layer and a Leaky ReLU layer), and each step is composed of a block and a max pooling layer. Meanwhile, the decoder part consists of four upsampling steps, a block and a sigmoid activation function layer. Each upsampling step is made up of a block and an upsampling layer.

5.2 Adaptive Denoising Architecture

Indeed, we can directly perform Eq. (8) to realize the low-light image enhancement. However, this way implicitly contains an assumption, i.e., noises/artifacts do not exist in the reflectance. It will cause uncontrollable performance in some unknown and challenging low-light scenarios (maybe exist noises/artifacts). To handle these scenarios, we further construct a denoising mechanism which can be described as

$$\hat{\mathbf{z}} = \mathbf{z} - \mathcal{G}(\mathbf{z}; \Theta_{\mathcal{G}}), \quad (9)$$

where $\hat{\mathbf{z}}$ represents the final output after denoising. \mathcal{G} represents the noise estimation network with the parameters $\Theta_{\mathcal{G}}$, whose architecture contains five convolutional layers, and each of the layer is followed by a ReLU activation function layer. An estimated noise map is generated by the module. Then the denoising effect can be achieved by subtracting the enhanced image from the noise map.

Actually, as for training \mathcal{G} , we can directly adopt image pairs (low-light input contains noises) to train it. But if doing this, the model just addresses this case and loses the generalization. To this end, we propose to establish an adaptive denoising model by introducing a new adversarial loss for different types of data. The specific form of this loss function can be found in the upcoming section.

5.3 Training Loss for Brightening Process

Here, we define two types of training loss for brightening from the data perspective. If the targeted datasets contain the reference images, we can utilize the supervised loss. Otherwise, we adopt the unsupervised loss to satisfy the case of no reference images.

Supervised Loss. We utilize the following MSE loss to train the brightening architecture so as to improve the enhancement capability.

$$\mathcal{L}_{\text{su}} = \|\mathbf{z} - \mathbf{z}_{\text{gt}}\|^2, \quad (10)$$

where \mathbf{z} represents the reflection obtained by the encoder-decoder estimation of the input image, while \mathbf{z}_{gt} represents the ground truth image.

Unsupervised Loss. The more common and challenging scenes are that the datasets only contain low-light observations, without the corresponding reference images. In this case, we adopt the unsupervised training loss following the work in (Liu et al. 2021d), represented as

$$\mathcal{L}_{\text{uns}} = \lambda \|\mathbf{x} - \mathbf{y}\|^2 + \sum_{i=1}^N \sum_{j \in \mathcal{N}(i)} w_{i,j} |\mathbf{x}_i^t - \mathbf{x}_j^t|, \quad (11)$$

where the first and second terms are fidelity and smoothing loss, respectively. The fidelity loss aims to guarantee the pixel-level consistency of the low-light input \mathbf{y} and illumination \mathbf{x} . As for the smoothing loss, we adopt the spatially-variant ℓ_1 -norm (Fan et al. 2018) as the smoothness term in this paper, where N and i indicate the total number of pixels and the i -th pixel. $w_{i,j}$ represents the weight, whose formulated form is $w_{i,j} = \exp\left(-\frac{\sum_c ((\mathbf{y}_{i,c} + \mathbf{s}_{i,c}^{t-1}) - (\mathbf{y}_{j,c} + \mathbf{s}_{j,c}^{t-1}))^2}{2\sigma^2}\right)$, where c denotes image channel in the YUV color space. $\sigma = 0.1$ is the standard deviations for the Gaussian kernels. The hyper-parameter λ is empirically set to 0.2.

5.4 Adversarial Loss for Denoising Process

During the training process, in order to obtain the capability of adaptive denoising, we utilize a dataset with noisy images (e.g., LOL) and a dataset without noise (e.g., MIT) to train the network. We aim to obtain a denoising network with the ability to automatically identify noise. The denoising module distinguishes images that generated by the previous networks. Nevertheless, the previous encoder and decoder are trained noise-insensitive (not care if there is noise on the input image), which significantly increase the difficulty of identifying noise for the denoising module. Therefore, we need a reliable training loss to guide the denoising module.

Following the manner presented in (Sindagi et al. 2020), we define a new adversarial loss to learn an adaptive denoising module, which is able to distinguish image with/without

Table 2 Quantitative results (Metrics with reference: PSNR, SSIM, and LPIPS; Metrics without reference: DE, LOE, and NIQE) on MIT and LOL datasets. The best result is in bold red whereas the second best one is in bold blue.

Metrics		RetinexNet	DeepUPE	KinD	EnGAN	FIDE	DRBN	ZeroDCE	RUAS	UTVNet	SCL	BL	RBL
MIT	PSNR↑	12.9500	18.3862	16.2148	15.3271	14.9522	15.2089	15.5432	18.5549	16.3470	16.4040	20.1299	20.6759
	SSIM↑	0.5996	0.7922	0.7243	0.7247	0.6489	0.6684	0.7232	0.7683	0.7351	0.7721	0.8413	0.8352
	LPIPS↓	0.3654	0.1970	0.2535	0.2376	0.3368	0.3153	0.2191	0.1721	0.2214	0.1881	0.1799	0.1631
	DE↑	6.1320	7.0559	6.6879	7.0327	6.7724	6.6012	6.2838	7.2471	6.6270	6.2947	7.2521	7.3109
	LOE↓	1206.40	187.73	502.84	844.57	552.99	678.45	475.23	341.22	272.64	563.90	183.42	171.09
	NIQE↓	5.6853	4.1581	4.5200	5.0463	5.5359	5.0958	4.2899	4.1312	4.4722	4.0044	4.0318	4.4554
LOL	PSNR↑	14.2995	18.1951	17.3540	15.3148	18.9835	19.3976	18.4158	16.0052	20.0077	15.4014	20.4271	20.6905
	SSIM↑	0.4965	0.6617	0.7181	0.6163	0.7518	0.7223	0.7245	0.6803	0.8565	0.6644	0.7331	0.7728
	LPIPS↓	0.5429	0.3383	0.1518	0.3088	0.2141	0.2520	0.3126	0.2384	0.2891	0.3004	0.1305	0.1443
	DE↑	6.9049	6.1240	7.2118	6.9634	6.5978	6.9074	6.6565	6.9763	6.7385	6.3470	6.6595	7.0123
	LOE↓	857.25	228.41	481.32	551.13	1410.60	619.19	204.56	326.82	346.78	239.48	314.77	285.61
	NIQE↓	9.4275	7.5147	4.8798	5.0888	4.9493	4.5934	5.0578	4.6483	5.4438	7.7964	4.5289	4.5554

noises. This loss can be formulated as

$$\mathcal{L}_{adv}^l = \|\hat{\mathbf{z}}^l - \mathbf{z}_{gt}^l\|^2, l = a, b, \quad (12)$$

where $\{\hat{\mathbf{z}} = \hat{\mathbf{z}}^a \cup \hat{\mathbf{z}}^b, \mathbf{z}_{gt} = \mathbf{z}_{gt}^a \cup \mathbf{z}_{gt}^b\}$ represents that the training pairs $\{\mathbf{z}, \mathbf{z}_{gt}\}$ can be split to two groups, i.e., low-light image pairs with noises $\{\mathbf{z}^a, \mathbf{z}_{gt}^a\}$ and low-light image pairs without noises $\{\mathbf{z}^b, \mathbf{z}_{gt}^b\}$.

6 Experimental Results

In this section, we first introduced the implementation details related to the experiments. Subsequently, aiming to comprehensively validate the superiority of our method, we provided subjective and objective comparison results and analysis between the proposed method and state-of-the-art methods in the field, conducted in multiple testing cases, including seen-paired, unseen-paired, unseen-unpaired datasets.

6.1 Implementation Details

Here, we introduced implementation details from three aspects, including benchmarks description, compared methods and metrics, and parameters setting.

Benchmarks description. We adopted five representative datasets (including MIT (Bychkovsky et al. 2011b), LOL (Chen et al. 2018), LSRW (Hai et al. 2021), VOC (Lv et al. 2021), DARKFACE (Yang et al. 2020)) to comprehensively evaluate the performance. As shown in Table 1, we executed the learning phase (BL and RBL) by using MIT (without noises) and LOL (with noises) datasets to define $\Theta_{\mathcal{F}_E}$ and Θ_G . Then all four datasets were performed in the adaptation (for defining $\Theta_{\mathcal{F}_p}$) and testing phases. The

adopted numbers of different stages for each dataset were also reported in Table 1. Notice that we used the same setting in the learning and adaptation stages. Finally, we also made evaluations on some challenging scenarios.

Compared methods and metrics. We compared the proposed method with a series of recently proposed state-of-the-art approaches, including RetinexNet (Chen et al. 2018), DeepUPE (Wang et al. 2019b), KinD (Zhang et al. 2019), EnGAN (Jiang et al. 2021), UTVNet (Zheng et al. 2021), ZeroDCE (Li et al. 2021), FIDE (Xu et al. 2020), SCL (Liang et al. 2022), RUAS (Liu et al. 2021d). We utilized several mainstream metrics with reference (including PSNR, SSIM, and LPIPS (Zhang et al. 2018b)), and metrics without reference (including DE (Shannon 1948), LOE (Wang et al. 2013) and NIQE (Mittal et al. 2012)) to measure the quality of output images.

Parameters setting. During the learning and adaptation phases, we used the ADAM optimizer (Kingma and Ba 2014) with parameters $\beta_1 = 0.5$, $\beta_2 = 0.999$, and $\epsilon = 1 \times 10^{-3}$. The minibatch size was set to 8 and learning rate was initialized to 1×10^{-3} . Besides, all our experiments was completed with PyTorch framework on NVIDIA TITAN XP.

6.2 Evaluations on Seen-Paired Benchmarks

In this part, we aimed at verifying the effectiveness of our proposed method in a series of standard datasets which contained the reference images. The first part provided numerical results on datasets that were used for learning, it follows the regular pattern, i.e., acquiring the overall parameters by using the same data distribution with the testing phase. The second part presented related subjective results.

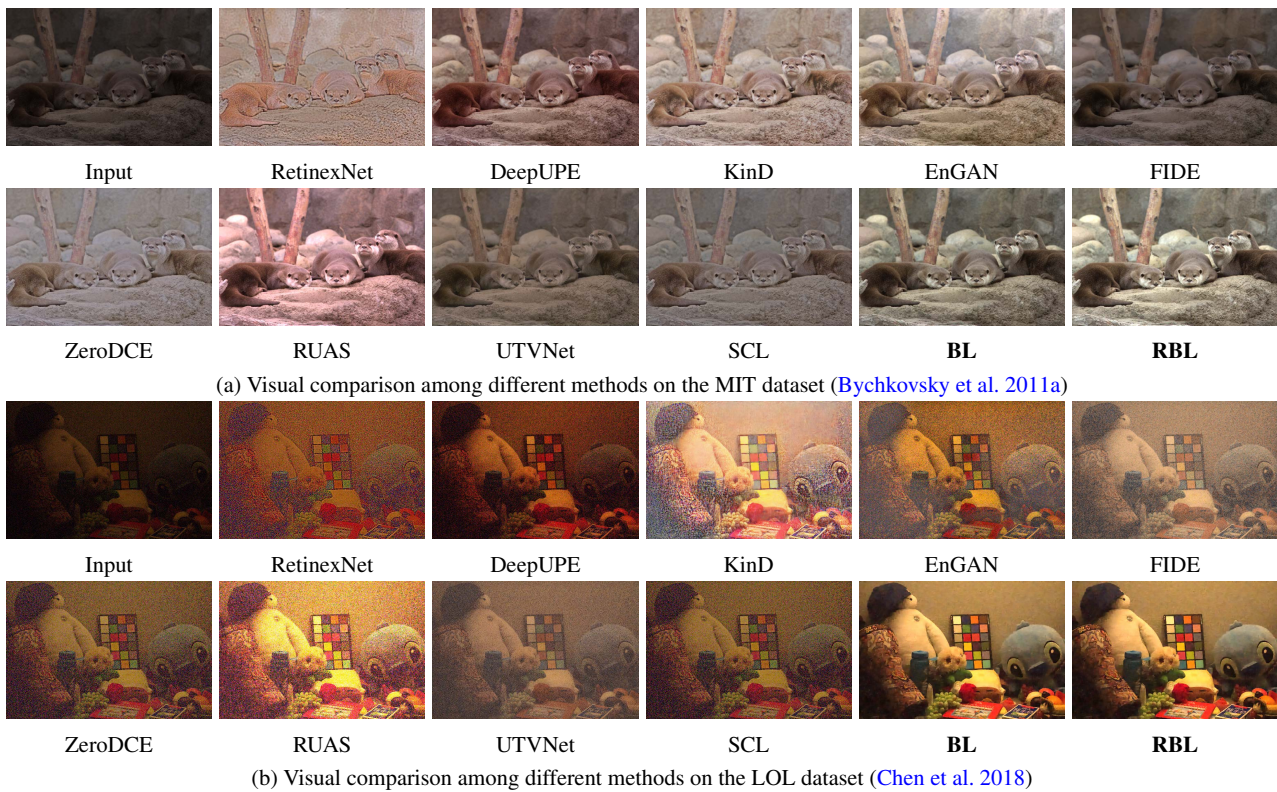


Fig. 6 Visual results of state-of-the-art methods and our two versions (BL and RBL) on different datasets.

Quantitative comparison. First and foremost, quantitative results on the MIT and LOL datasets were reported in Table 2. It is evident that the proposed BL and RBL methods consistently achieved top rankings (almost all are the best or second best) in the majority of the performance metrics among other methods. Furthermore, the proposed extended version demonstrated significant performance improvement compared to BL, providing evidence of the effectiveness and superiority of the reinforced bilevel learning scheme.

Qualitative comparison. Visual comparison with state-of-the-art methods were presented in Fig. 6. It could be seen that the results of other methods exhibit noticeable underexposure or overexposure. Some methods (RetinexNet and RUAS) even demonstrated color distortion issues. In comparison, our method achieved superior performance on the MIT dataset, demonstrating more appropriate brightness and color in contrast to other methods. Furthermore, the results on the LOL dataset provided evidence that the proposed method significantly removed noise and exhibits clear advantages over the comparative methods.

6.3 Evaluations on Unseen-Paired Benchmarks

To demonstrate the generalization capability of our method, we compared the proposed method with the state-of-the-art approaches on other datasets which contained the reference.

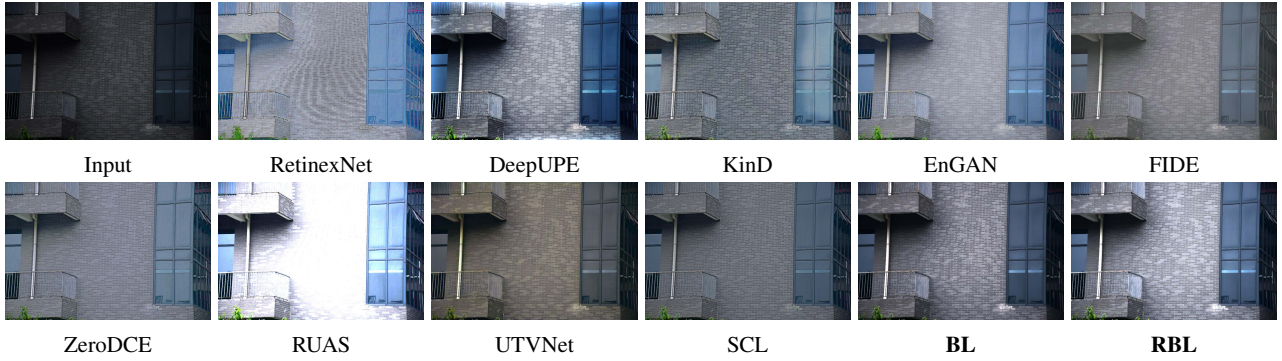
It is noteworthy that the quantitative results provided in the first part differed from the conventional setting, as the testing phase utilized completely new data with a distinct distribution compared to the learning phase.

Quantitative comparison. As shown in Table 3, although testing on unseen scenarios had somewhat affected the advantages of our method, it still maintained a competitive performance. Furthermore, regarding the results of our two proposed versions, the RBL outperformed the original scheme in the most of performance metrics. The aforementioned phenomenon provided evidence that by introducing optimization measures for the initial values of the decoder, we had indeed achieved a more beneficial initialization, enabling it to fast adapt to different scenarios.

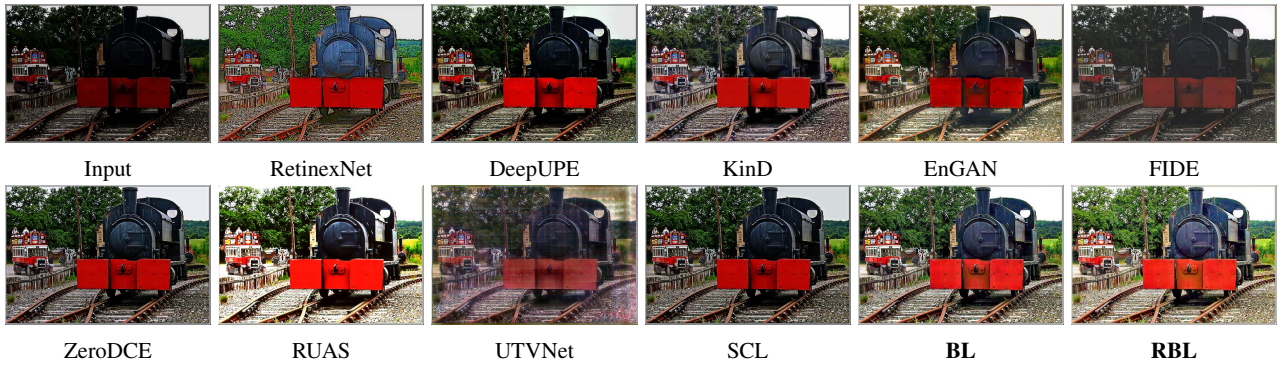
Qualitative comparison. The results of our method and other approaches on the LSRW and VOC datasets were presented in Fig. 7. From Fig. 7 (a), it could be seen that other methods exhibited poor performance on the LSRW dataset. RUAS suffered from overexposure, while EnGAN and FIDE exhibited noticeable underexposure. Additionally, RetinexNet disrupted the details and textures, and UTVNet not only had underexposure but also exhibited color shifts. From the results in Fig. 7 (b), it is also obvious that UTVNet exhibited noticeable artifacts. In contrast, the enhancement results of our BL and RBL not only achieved optimal lighting intensity but also outperformed other methods signifi-

Table 3 Quantitative results (Metrics with reference: PSNR, SSIM, and LPIPS; Metrics without reference: DE, LOE, and NIQE) on LSRW and VOC datasets. The best result is in bold red whereas the second best one is in bold blue.

Metrics		RetinexNet	DeepUPE	KinD	EnGAN	FIDE	DRBN	ZeroDCE	RUAS	UTVNet	SCL	BL	RBL
LSRW	PSNR \uparrow	15.9062	16.8890	16.4717	16.3106	17.6694	16.1497	15.8337	14.4372	16.4771	16.1327	14.8726	15.3892
	SSIM \uparrow	0.3725	0.5125	0.4929	0.4697	0.5485	0.5422	0.4664	0.4276	0.6673	0.5710	0.5933	0.6761
	LPIPS \downarrow	0.4326	0.3466	0.3371	0.3299	0.3351	0.3347	0.3174	0.3726	0.2913	0.3623	0.3844	0.3633
	DE \uparrow	6.9392	6.7712	7.0368	6.6692	6.8745	7.2051	6.8729	5.6056	7.0330	6.4815	6.8634	6.8293
	LOE \downarrow	591.28	339.02	379.90	248.19	221.94	755.13	219.13	357.41	219.45	235.80	255.79	215.92
	NIQE \downarrow	4.1479	3.9816	3.6636	3.7754	4.3277	4.5500	3.7183	4.1687	4.0145	3.8422	4.0179	3.5265
VOC	PSNR \uparrow	15.4087	15.7017	16.3160	10.7134	15.8569	15.7868	14.1782	17.0125	16.9024	14.8902	16.7280	17.1492
	SSIM \uparrow	0.5971	0.5619	0.6564	0.2985	0.6101	0.5209	0.4412	0.6738	0.6539	0.5516	0.6325	0.6477
	LPIPS \downarrow	0.2489	0.2260	0.2260	0.2073	0.4002	0.2165	0.3034	0.3852	0.2239	0.1797	0.1987	0.2103
	DE \uparrow	7.2555	6.6517	7.2906	5.7221	7.0681	6.8160	6.7553	6.9088	7.2089	6.3099	6.9586	6.8790
	LOE \downarrow	845.26	485.59	389.41	311.41	408.34	591.20	423.78	340.24	423.47	435.74	246.98	233.04
	NIQE \downarrow	6.0860	5.0727	4.6222	5.1635	5.7456	4.7397	4.8665	4.7712	4.7071	4.8824	5.3080	4.8916



(a) Visual comparison among different methods on the LSRW dataset (Hai et al. 2021)



(b) Visual comparison among different methods on the VOC dataset (Lv et al. 2021)

Fig. 7 Visual results of state-of-the-art methods and our two versions (BL and RBL) on different datasets.

cantly in terms of both color and texture details, highlighting the advantages of the proposed approach. The enhanced visual appeal of RBL compared to BL further validated the effectiveness of RBL. Besides, more subjective results on four datasets in Fig. 8 further illustrated our advantages. The first four rows of results demonstrated that our method produced more suitable lighting and vivid colors while effectively handling scenarios with significant noise. The latter

two rows of results indicated that our method exhibited good generalization capability by adapting well to unseen scenes.

6.4 Evaluations on Unseen-Unpaired Benchmarks

We conducted a series of comparative experiments on two challenging unpaired datasets to further demonstrate the fast adaptability of our method in extreme low-light conditions.

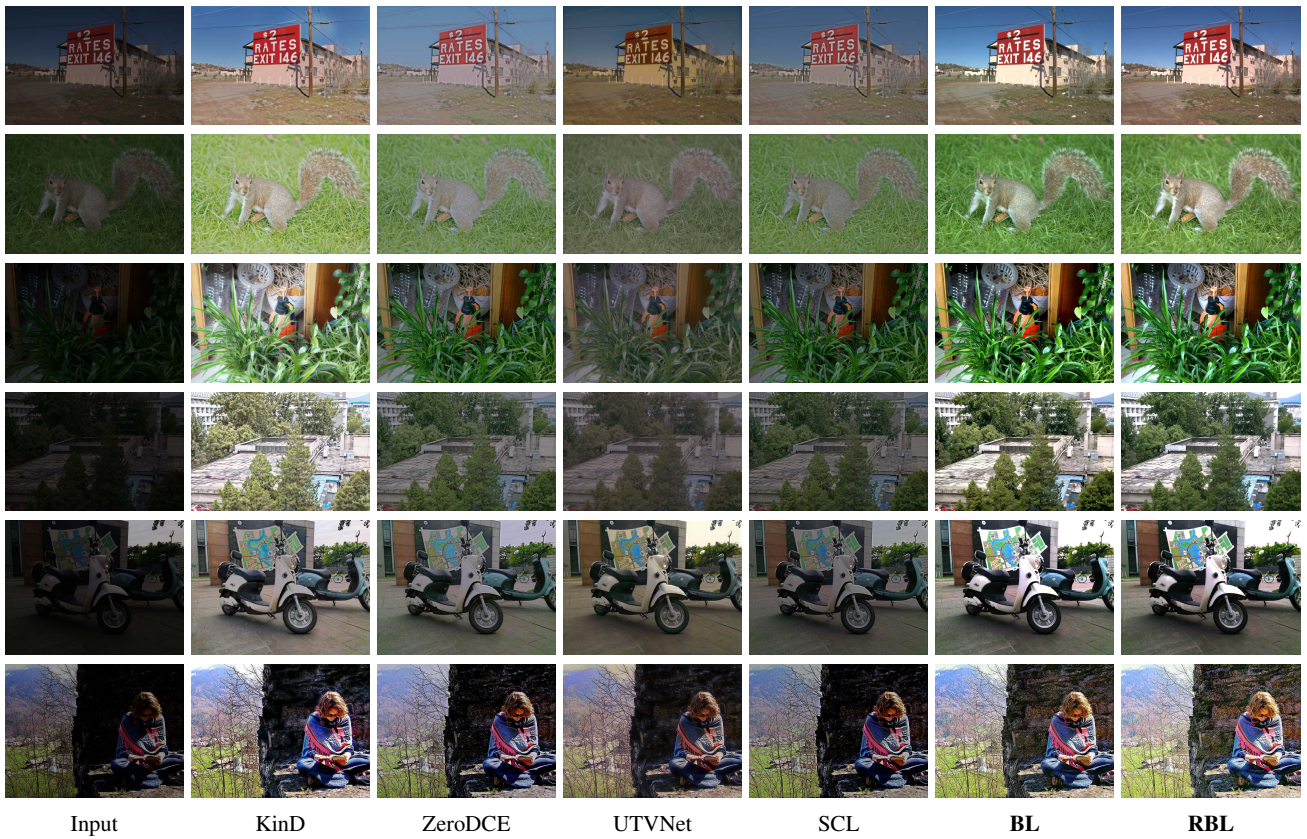


Fig. 8 More visual comparisons on the standard datasets. The top two and middle two rows come from the MIT and LOL datasets, respectively. The last two rows come from the LSRW and VOC datasets, respectively.

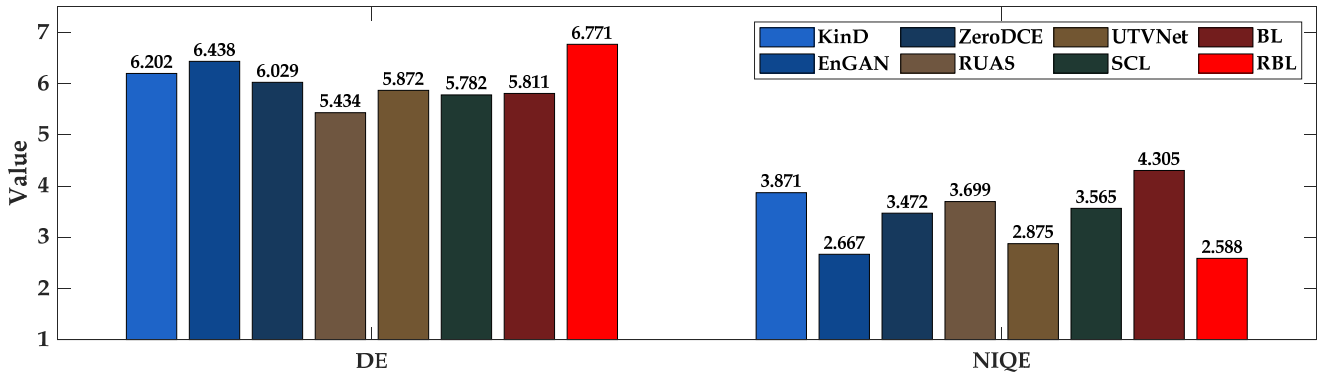


Fig. 9 Numerical scores (DE \uparrow and NIQE \downarrow) among different state-of-the-art methods and our two versions on the DARK FACE dataset.

The testing protocol used in this section remains consistent with Section 6.3.

Quantitative comparison. As illustrated by the numerical results shown in Fig. 9, the proposed RBL achieved significant improvements over BL in both DE and NIQE, outperforming other methods and demonstrating that our method could obtain the enhancement results whose texture detail and color were more in line with human visual habits.

Qualitative comparison. The three sets of qualitative results presented in Fig. 10 revealed a common issue of un-

derexposure in the compared methods. In contrast, our method significantly improved image brightness and better preserved texture details. Further, we tested our algorithm on the Exclusively Dark (ExDARK) (Loh and Chan 2018) dataset, an unpaired challenging dataset constructed by collecting low-light images from different datasets with object class annotation. As Fig. 11 illustrated, although the other methods achieved brightness enhancement, their results still exhibited a significant amount of noticeable noise. In contrast, our method could effectively brighten the image while ensuring

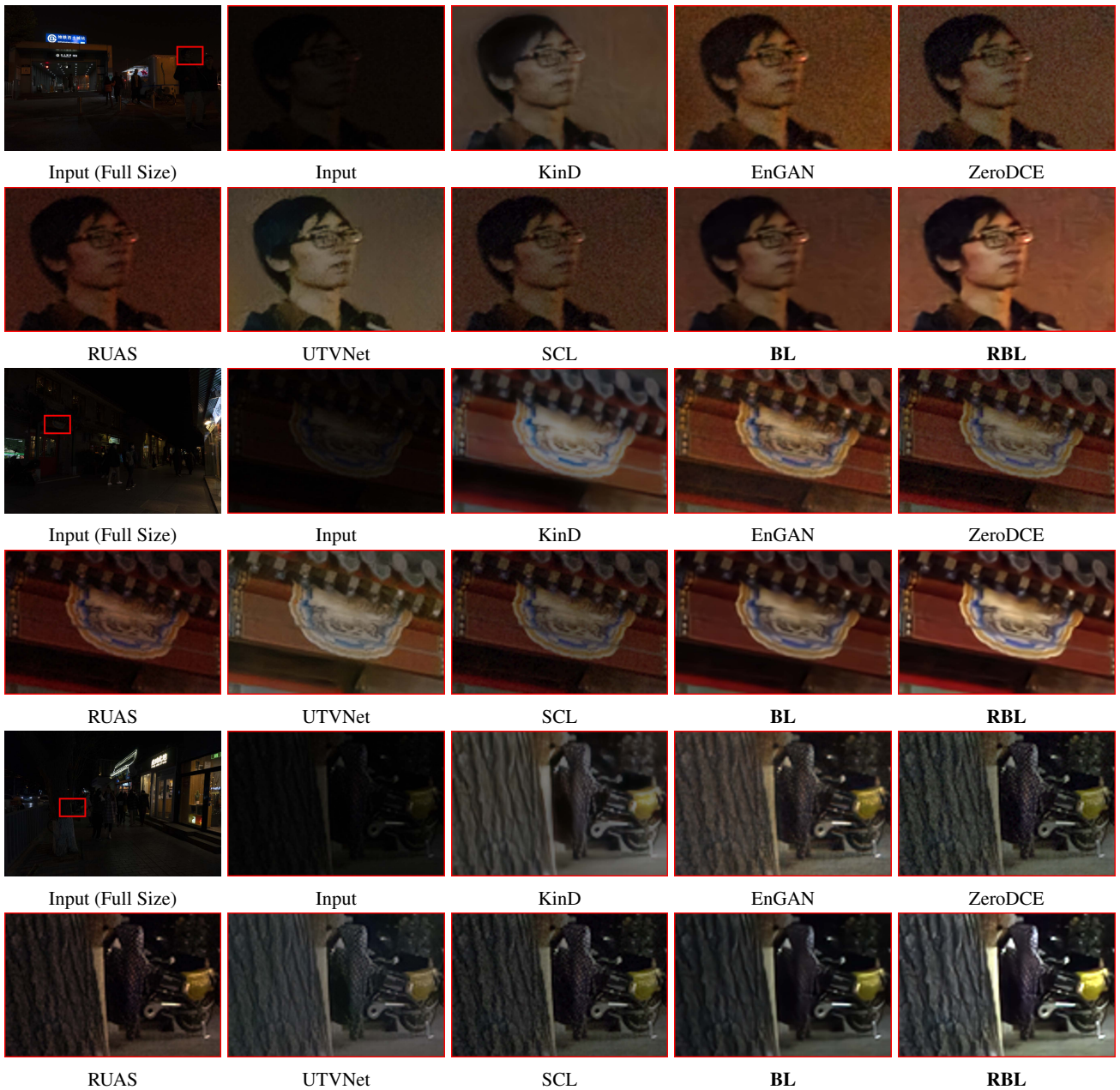


Fig. 10 Visual results of state-of-the-art methods and our two versions (BL and RBL) on the DARKFACE dataset.

that the noise in the image was removed to a certain extent. It proved that our method could not only adapt to different scenes in illumination estimation, but also achieve good results in denoising at the same time.

7 Algorithmic Analyses

In this section, we provided a series of algorithm analyses to validate the effectiveness of the proposed bilevel optimization framework. We first analyze the effect of different learning strategies by comparing the performance of the naive

scheme and our method in terms of convergence. Subsequently, we analyze the advantages of the reinforced bilevel learning framework. Last but not least, we provide relevant results from ablation experiments on the employed finetuning strategy and the role of the constructed adaptive denoising module.

7.1 Bilevel Learning vs Naive Learning

Fig. 12 displayed the results of our training strategies compared to naive strategies. Both strategies were trained on a

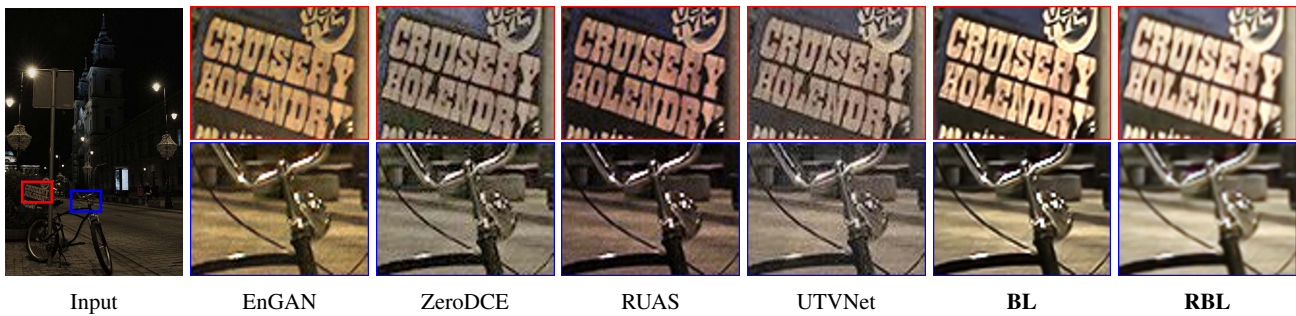


Fig. 11 Visual results of state-of-the-art methods and our two versions (BL and RBL) on the ExDARK dataset.

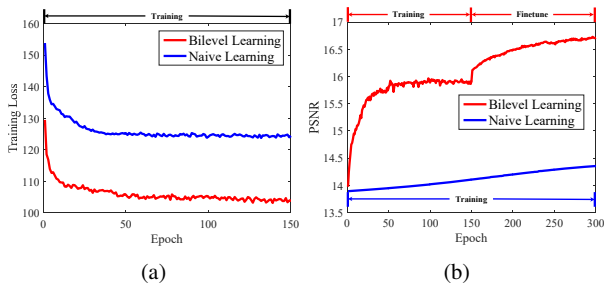


Fig. 12 Convergence behaviors of naive learning and our method. (a) is the loss comparison when both of them are trained with mixed datasets of MIT and LOL. (b) is the PSNR comparison of our training strategy and naive approach (training with a single dataset (VOC) only). As for the second graph, we execute the bilevel training for 150 epochs and finetuning for another 150 epochs, and train the naive approach for 300 epochs to ensure fairness.

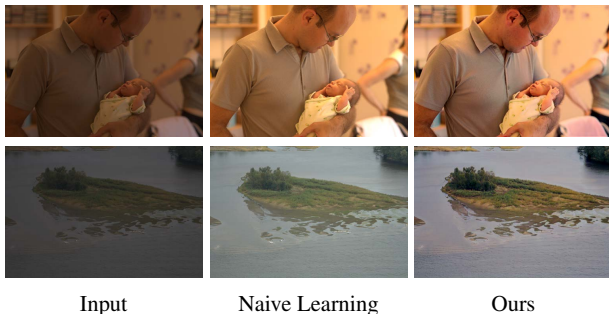


Fig. 13 Visual comparison among different training strategy on the MIT dataset. Ours are better than naive both on color and exposure.

mixed dataset of the MIT and LOL datasets and tested on 100 randomly selected images from the VOC dataset. In each experiment, 300 epochs were trained in naive steps to ensure fairness. The results showed that the training loss, PSNR values of naive method were not as outstanding as our strategy. It is proved that the model generated by ours strategy possessed faster convergence speed and stronger generalization ability. As is shown in Fig. 13, we tested our algorithm and naive methods on MIT dataset, and it is obvious that the proposed method took both illumination and color information into account.

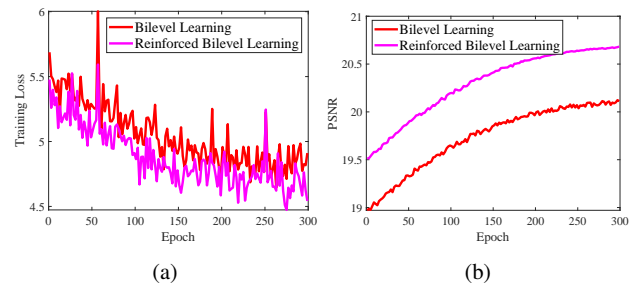


Fig. 14 Convergence behaviors of our two versions in the adaptation stage on the MIT dataset. (a) is the loss comparison. (b) is the PSNR value comparison.

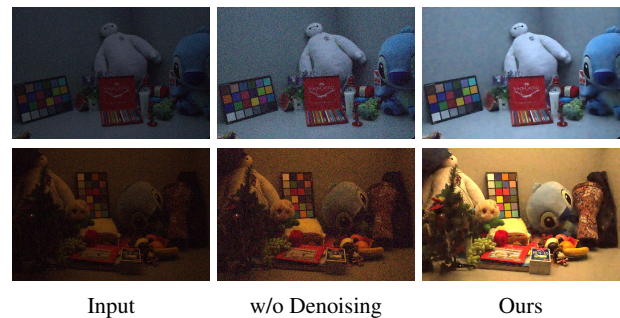


Fig. 15 Ablation study of denoise module. The result with denoising module is not only brighter but also clearer, which proves the effectiveness of our denoising module.

7.2 Bilevel Learning vs Reinforced Bilevel Learning

The comparative results regarding the convergence of the newly proposed RBL and BL were presented in Fig. 14. The experimental setup for this analysis was largely consistent with Section 7.2, with the difference that we only presented the results from the adaptation phase to analyze the advantages of RBL. It is evident that RBL exhibited significant advantages over the original version in terms of both loss convergence and performance improvement. It indicated that with the reinforced bilevel learning strategy, we could further improve the convergence rate and obtain initializations, resulting in faster adaptation.



Fig. 16 Ablation study of finetune process.

Table 4 Effects of denoising module and finetune mechanism.

Effects of denoising on the LOL dataset			
Model	PSNR	SSIM	LPIPS
w/o Adaptive Denoising	11.1692	0.2750	1.1439
w/ Adaptive Denoising	15.4120	0.4205	0.5444
Effects of finetune on the VOC dataset			
Model	PSNR	SSIM	LPIPS
w/o Finetune	15.7692	0.6181	0.2503
w/ Finetune	16.7280	0.6325	0.1987

7.3 Effects of Adaptive Denoising

We presented the visual results of the ablation experiment on the adaptive denoising module in Fig. 15. It is evident that when the adaptive denoising module is removed, significant noise artifacts appear in the enhanced results, indicating that the network loses its ability to remove noise. This is because the network we constructed can accurately estimate the noise map. The relevant numerical results presented in Table 4 also demonstrated that the removal of the adaptive denoising module had a significant negative impact on the practical metric, which further verified its effectiveness.

7.4 Effects of Finetune Process

As for the finetune period shown in Fig. 16, we only utilized 250 images from VOC to train 30 epochs. It could be observed that although the images without finetune could still recover part of the original image information, the illumination estimation after finetune seemed to be more accurate. The quantitative comparison of the finetuning strategy in Table 4 can also show its positive effect. It is proved that a small amount of finetune could significantly improve effects.



Fig. 17 Intermediate results, including illumination x , enhanced image before denoising z , noise map $G(z; \Theta_G)$ after normalization, and final output \hat{z} .

7.5 Intermediate Results

Last but not least, we displayed the intermediate results of our proposed network in Fig. 17. Although we did not use a certain loss to constrain the illumination, it still seems smooth. Also, the noise map did not contain much marginal information. That is to say, after going through the denoising module, the original image would not be blurred much edge information. Thus, it proved that our training strategy is helpful for the whole network to generate the original properties of every intermediate result, which played a pivotal role in recovering sufficiently accurate image information.

8 Conclusions and Future Works

In this study, we proposed a bilevel learning framework for low-light image enhancement to achieve fast adaptation towards different scenes. We explored the underlying relationships among low-light scenes and modeled them from hyperparameter optimization, which enabled us to obtain a scene-independent general encoder. Then we defined a bilevel learning framework to acquire a frozen encoder in the subsequent phases. Furthermore, we designed a reinforced bilevel learning framework to provide the meta-initialization for decoder to further improve the visual quality. Last but not least, a Retinex-induced framework capable of adaptive denoising had been constructed to enhance the practicality of the algorithm, and we applied the proposed learning scheme under different training constraints including supervised and unsupervised forms. A series of evaluated experiments and algorithm analyses were conducted under different scenes thoroughly validated our superiority and effectiveness.

In the future, we will try our best to continue exploring the fast adaptation ability for more computer vision tasks from the perspective of hyperparameter optimization. Moreover, another direction to pay more attention is how to endow fast adaptation ability towards unseen scenes for lightweight or high-efficient models.

Acknowledgements This work was supported by the National Natural Science Foundation of China (Nos. U22B2052, 62027826), the LiaoNing Revitalization Talents Program (No. 2022RG04).

References

- Bychkovsky V, Paris S, Chan E, Durand F (2011a) Learning photographic global tonal adjustment with a database of input / output image pairs. In: The Twenty-Fourth IEEE Conference on Computer Vision and Pattern Recognition **2, 9**
- Bychkovsky V, Paris S, Chan E, Durand F (2011b) Learning photographic global tonal adjustment with a database of input/output image pairs. In: Proceedings of the IEEE/CVF Conference on Computer Vision and Pattern Recognition, pp 97–104 **2, 4, 8**
- Chen W, Wang W, Yang W, Liu J (2018) Deep retinex decomposition for low-light enhancement. In: British Machine Vision Association **1, 2, 4, 8, 9**
- Chi Z, Wang Y, Yu Y, Tang J (2021) Test-time fast adaptation for dynamic scene deblurring via meta-auxiliary learning. In: Proceedings of the IEEE/CVF Conference on Computer Vision and Pattern Recognition, pp 9137–9146 **2, 3**
- Choi M, Choi J, Baik S, Kim TH, Lee KM (2021) Test-time adaptation for video frame interpolation via meta-learning. *IEEE Transactions on Pattern Analysis and Machine Intelligence* **4, 5**
- Cui Z, Qi GJ, Gu L, You S, Zhang Z, Harada T (2021) Multitask aet with orthogonal tangent regularity for dark object detection. In: Proceedings of the IEEE/CVF International Conference on Computer Vision, pp 2553–2562 **1**
- Falkner S, Klein A, Hutter F (2018) Bohb: Robust and efficient hyperparameter optimization at scale. In: International Conference on Machine Learning, PMLR, pp 1437–1446 **5**
- Fan Q, Yang J, Wipf D, Chen B, Tong X (2018) Image smoothing via unsupervised learning. *ACM Transactions on Graphics* 37(6):1–14 **7**
- Feurer M, Hutter F (2019) Hyperparameter optimization. In: Automated Machine Learning, Springer, Cham, pp 3–33 **5**
- Finn C, Abbeel P, Levine S (2017) Model-agnostic meta-learning for fast adaptation of deep networks. In: International Conference on Machine Learning, pp 1126–1135 **2, 3**
- Franceschi L, Frasconi P, Salzo S, Grazzi R, Pontil M (2018) Bilevel programming for hyperparameter optimization and meta-learning. In: International Conference on Machine Learning, PMLR, pp 1568–1577 **5**
- Gao H, Guo J, Wang G, Zhang Q (2022a) Cross-domain correlation distillation for unsupervised domain adaptation in nighttime semantic segmentation. In: Proceedings of the IEEE/CVF Conference on Computer Vision and Pattern Recognition, pp 9913–9923 **1**
- Gao Z, Wu Y, Harandi MT, Jia Y (2022b) Curvature-adaptive meta-learning for fast adaptation to manifold data. *IEEE Transactions on Pattern Analysis and Machine Intelligence* **3**
- Gu J, Wang Z, Kuen J, Ma L, Shahroudy A, Shuai B, Liu T, Wang X, Wang G, Cai J, et al. (2018) Recent advances in convolutional neural networks. *Pattern Recognition* 77:354–377 **1**
- Guo C, Li C, Guo J, Loy CC, Hou J, Kwong S, Cong R (2020) Zero-reference deep curve estimation for low-light image enhancement **3**
- Guo X, Li Y, Ling H (2017) Lime: Low-light image enhancement via illumination map estimation. *IEEE Transactions on Image Processing* 26(2):982–993 **6**
- Hai J, Xuan Z, Yang R, Hao Y, Zou F, Lin F, Han S (2021) R2rnet: Low-light image enhancement via real-low to real-normal network. *arXiv preprint arXiv:210614501* **2, 8, 10**
- Jiang Y, Gong X, Liu D, Cheng Y, Fang C, Shen X, Yang J, Zhou P, Wang Z (2021) Enlightengan: Deep light enhancement without paired supervision. *IEEE Transactions on Image Processing* 30:2340–2349 **1, 3, 8**
- Jin D, Ma L, Liu R, Fan X (2021) Bridging the gap between low-light scenes: Bilevel learning for fast adaptation. In: Proceedings of the 29th ACM International Conference on Multimedia, pp 2401–2409 **2**
- Kingma DP, Ba J (2014) Adam: A method for stochastic optimization. In: International Conference on Learning Representations, pp 1–13 **8**
- Land EH, McCann JJ (1971) Lightness and retinex theory. *Journal of the Optical Society of America* **6**
- Lee S, Cho D, Kim J, Kim TH (2020) Self-supervised fast adaptation for denoising via meta-learning. *arXiv preprint arXiv:200102899* **2, 3, 4, 5**
- Li C, Guo C, Chen CL (2021) Learning to enhance low-light image via zero-reference deep curve estimation. *IEEE Transactions on Pattern Analysis and Machine Intelligence* **1, 8**
- Liang D, Li L, Wei M, Yang S, Zhang L, Yang W, Du Y, Zhou H (2021a) Semantically contrastive learning for low-light image enhancement. In: Proceedings of the AAAI Conference on Artificial Intelligence **3**
- Liang D, Li L, Wei M, Yang S, Zhang L, Yang W, Du Y, Zhou H (2022) Semantically contrastive learning for low-light image enhancement. In: Proceedings of the AAAI Conference on Artificial Intelligence, vol 36, pp 1555–1563 **2, 8**
- Liang J, Wang J, Quan Y, Chen T, Liu J, Ling H, Xu Y (2021b) Recurrent exposure generation for low-light face detection. *IEEE Transactions on Multimedia* 24:1609–1621 **1**
- Liu H, Simonyan K, Yang Y (2018) Darts: Differentiable architecture search. In: International Conference on Learning Representations **5**
- Liu H, Wu Z, Li L, Salehkalaibar S, Chen J, Wang K (2022) Towards multi-domain single image dehazing via test-time training. In: Proceedings of the IEEE/CVF Conference on Computer Vision and Pattern Recognition, pp 5831–5840 **3, 4, 5**
- Liu R, Mu P, Chen J, Fan X, Luo Z (2020a) Investigating task-driven latent feasibility for nonconvex image modeling. *IEEE Transactions on Image Processing* 29:7629–7640 **5**
- Liu R, Mu P, Yuan X, Zeng S, Zhang J (2020b) A generic first-order algorithmic framework for bi-level programming beyond lower-level singleton. In: International Conference on Machine Learning, PMLR, pp 6305–6315 **5**
- Liu R, Gao J, Zhang J, Meng D, Lin Z (2021a) Investigating bi-level optimization for learning and vision from a unified perspective: A survey and beyond. *IEEE Transactions on Pattern Analysis and Machine Intelligence* **2, 3, 5, 6**
- Liu R, Liu X, Yuan X, Zeng S, Zhang J (2021b) A value-function-based interior-point method for non-convex bi-level optimization. In: International Conference on Machine Learning, PMLR **5**
- Liu R, Liu Y, Zeng S, Zhang J (2021c) Towards gradient-based bilevel optimization with non-convex followers and beyond. *Advances in Neural Information Processing Systems* 34:8662–8675 **6**
- Liu R, Ma L, Zhang J, Fan X, Luo Z (2021d) Retinex-inspired unrolling with cooperative prior architecture search for low-light image enhancement. In: Proceedings of the IEEE/CVF Conference on Computer Vision and Pattern Recognition, pp 10561–10570 **7, 8**
- Loh YP, Chan CS (2018) Getting to know low-light images with the exclusively dark dataset. *arXiv:1805.11227* **2, 11**
- Lv F, Li Y, Lu F (2021) Attention guided low-light image enhancement with a large scale low-light simulation dataset. *International Journal of Computer Vision* 129(7):2175–2193 **2, 4, 8, 10**
- Ma L, Liu R, Zhang J, Fan X, Luo Z (2021) Learning deep context-sensitive decomposition for low-light image enhancement. *IEEE Transactions on Neural Networks and Learning Systems* **3**
- Ma L, Ma T, Liu R, Fan X, Luo Z (2022) Toward fast, flexible, and robust low-light image enhancement. In: Proceedings of the IEEE/CVF Conference on Computer Vision and Pattern Recognition, pp 5637–5646 **1, 3**
- Van der Maaten L, Hinton G (2008) Visualizing data using t-sne. *Journal of Machine Learning Research* 9(11) **3**

- Mittal A, Soundararajan R, Bovik AC (2012) Making a "completely blind" image quality analyzer. *IEEE Signal Processing Letters* 20(3):209–212 [8](#)
- Park S, Yoo J, Cho D, Kim J, Kim TH (2020) Fast adaptation to super-resolution networks via meta-learning. In: *European Conference on Computer Vision*, pp 754–769 [2](#), [3](#), [4](#), [5](#)
- Ronneberger O, Fischer P, Brox T (2015) U-net: Convolutional networks for biomedical image segmentation. In: *International Conference on Medical Image Computing and Computer Assisted Intervention*, pp 234–241 [4](#), [6](#)
- Sakaridis C, Dai D, Gool LV (2019) Guided curriculum model adaptation and uncertainty-aware evaluation for semantic nighttime image segmentation. In: *Proceedings of the IEEE/CVF International Conference on Computer Vision*, pp 7374–7383 [1](#)
- Shannon CE (1948) A mathematical theory of communication. *The Bell system technical journal* 27(3):379–423 [4](#), [8](#)
- Simon C, Koniusz P, Nock R, Harandi M (2020) Adaptive subspaces for few-shot learning. In: *Proceedings of the IEEE/CVF Conference on Computer Vision and Pattern Recognition*, pp 4136–4145 [5](#)
- Sindagi VA, Oza P, Yasarla R, Patel VM (2020) Prior-based domain adaptive object detection for hazy and rainy conditions. In: *European Conference on Computer Vision*, Springer, pp 763–780 [7](#)
- Vuorio R, Sun SH, Hu H, Lim JJ (2019) Multimodal model-agnostic meta-learning via task-aware modulation. *Advances in Neural Information Processing Systems* 32 [3](#)
- Wang R, Zhang Q, Fu CW, Shen X, Zheng WS, Jia J (2019a) Underexposed photo enhancement using deep illumination estimation. In: *Proceedings of the IEEE/CVF Conference on Computer Vision and Pattern Recognition* [3](#)
- Wang R, Zhang Q, Fu CW, Shen X, Zheng WS, Jia J (2019b) Underexposed photo enhancement using deep illumination estimation. In: *Proceedings of the IEEE/CVF Conference on Computer Vision and Pattern Recognition*, pp 6849–6857 [8](#)
- Wang S, Zheng J, Hu HM, Li B (2013) Naturalness preserved enhancement algorithm for non-uniform illumination images. *IEEE Transactions on Image Processing* 22(9):3538–3548 [4](#), [8](#)
- Wang S, Yang Y, Sun J, Xu Z (2021) Variational hyperadam: a meta-learning approach to network training. *IEEE Transactions on Pattern Analysis and Machine Intelligence* [3](#)
- Wang W, Wang X, Yang W, Liu J (2022) Unsupervised face detection in the dark. *IEEE Transactions on Pattern Analysis and Machine Intelligence* [1](#)
- Wu W, Weng J, Zhang P, Wang X, Yang W, Jiang J (2022) Uretinex-net: Retinex-based deep unfolding network for low-light image enhancement. In: *Proceedings of the IEEE/CVF Conference on Computer Vision and Pattern Recognition*, pp 5901–5910 [3](#)
- Wu X, Wu Z, Ju L, Wang S (2021) A one-stage domain adaptation network with image alignment for unsupervised nighttime semantic segmentation. *IEEE Transactions on Pattern Analysis and Machine Intelligence* [1](#)
- Xu K, Yang X, Yin B, Lau RW (2020) Learning to restore low-light images via decomposition-and-enhancement. In: *Proceedings of the IEEE/CVF Conference on Computer Vision and Pattern Recognition*, pp 2281–2290 [1](#), [2](#), [3](#), [8](#)
- Yang W, Yuan Y, Ren W, Liu J, Scheirer WJ, Wang Z, Zhang T, Zhong Q, Xie D, Pu S, et al. (2020) Advancing image understanding in poor visibility environments: A collective benchmark study. *IEEE Transactions on Image Processing* 29:5737–5752 [4](#), [8](#)
- Ye J, Fu C, Zheng G, Paudel DP, Chen G (2022) Unsupervised domain adaptation for nighttime aerial tracking. In: *Proceedings of the IEEE/CVF Conference on Computer Vision and Pattern Recognition*, pp 8896–8905 [1](#)
- Zhang Q, Yuan G, Xiao C, Zhu L, Zheng WS (2018a) High-quality exposure correction of underexposed photos. In: *ACM Multimedia*, pp 582–590 [6](#)
- Zhang R, Isola P, Efros AA, Shechtman E, Wang O (2018b) The unreasonable effectiveness of deep features as a perceptual metric. [arXiv:1801.03924](#) [8](#)
- Zhang Y, Zhang J, Guo X (2019) Kindling the darkness: A practical low-light image enhancer. In: *ACM Multimedia* [1](#), [3](#), [8](#)
- Zhang Z, Zheng H, Hong R, Xu M, Yan S, Wang M (2022) Deep color consistent network for low-light image enhancement. In: *Proceedings of the IEEE/CVF Conference on Computer Vision and Pattern Recognition*, pp 1899–1908 [3](#)
- Zhao L, Lu SP, Chen T, Yang Z, Shamir A (2021) Deep symmetric network for underexposed image enhancement with recurrent attentional learning. In: *Proceedings of the IEEE/CVF International Conference on Computer Vision*, pp 12075–12084 [3](#)
- Zheng C, Shi D, Shi W (2021) Adaptive unfolding total variation network for low-light image enhancement. In: *Proceedings of the IEEE/CVF International Conference on Computer Vision*, pp 4439–4448 [1](#), [3](#), [8](#)
- Ziko I, Dolz J, Granger E, Ayed IB (2020) Laplacian regularized few-shot learning. In: *International Conference on Machine Learning*, PMLR, pp 11660–11670 [5](#)